

1 **Fracturing of ductile anisotropic multilayers: influence of** 2 **material strength**

3

4 **E. Gomez-Rivas¹, A. Grier² and M.-G. Llorens³**

5 [1]{Department of Geology and Petroleum Geology, University of Aberdeen, Scotland,
6 United Kingdom}

7 [2]{Departament de Geologia, Universitat Autònoma de Barcelona, Spain}

8 [3]{Department of Geosciences, Eberhard Karls University of Tübingen, Germany}

9 Correspondence to: E. Gomez-Rivas (e.gomez-rivas@abdn.ac.uk)

10

11 **Abstract**

12 Fractures in rocks deformed under dominant ductile conditions typically form simultaneously
13 with viscous flow. Material strength plays a fundamental role on fracture development in such
14 cases, since fracture propagation can be strongly reduced by the **high energy absorption of the**
15 **material**. Additionally, the degree and nature of anisotropy can influence the orientation and
16 type of resulting fractures. In this study, four plasticine multilayer models have been
17 deformed under coaxial boundary conditions to investigate the influence of strength and
18 anisotropy on the formation of fracture networks. The experiments were made of different
19 mixtures and presented two types of anisotropy: composite and composite-intrinsic. The
20 transition from non-localised deformation to systems where fracture networks control
21 deformation accommodation is determined by the ability of the material to dissipate the
22 external work and relax the elastic strain during loading, either by viscous flow or by coeval
23 flow and failure. Tension cracks grow in experiments with composite anisotropy, giving rise
24 to a network of shear fractures when they collapse and coalesce with progressive deformation.
25 The presence of an additional intrinsic anisotropy enhances the direct nucleation of shear
26 fractures, whose propagation and final length depend on the rigidity of the medium. Material
27 strength increases the fracture maximum displacement (d_{max}) to fracture length (L) ratio, and
28 the resulting values are significantly higher than those from fractures in elastic-brittle rocks.

1 This is associated with the low propagation rates of fractures in rocks undergoing ductile
2 deformation.

3

4 **1 Introduction**

5 The deformation behaviour of Earth's crust rocks is often seen as a transition from frictional
6 and elastic-brittle behaviour at shallow depths to ductile crystal-plastic flow at deeper levels.
7 The change from brittle and discontinuous deformation (i.e. fracture-dominated) to ductile and
8 continuous deformation (i.e. flow-dominated) is known as the brittle-to-ductile transition, and
9 is typically characterised by systems in which displacement is accommodated by networks of
10 shear zones where brittle and ductile deformation coexist and compete (e.g. Paterson, 1978;
11 Passchier, 1984; Hobbs et al., 1986; Mancktelow, 2008a). It is assumed that an increase in
12 depth progressively reduces pressure-dependent plasticity and increases viscous flow, which
13 is mainly controlled by strain rate and temperature (e.g. ~~Mancktelow, 2006~~). However, field
14 observations and experiments suggest that coeval fracturing and rock flow are not restricted to
15 a certain zone in the middle crust, but can affect rocks at a wide range of depths and
16 deformation conditions from the Earth's surface to the upper mantle (e.g. Simpson, 1985;
17 Pennacchioni and Cesare, 1997; Guermani and Pennacchioni, 1998; Mancktelow 2009).
18 Moreover, brittle fractures can be precursors of ductile shear zones in certain cases (e.g.
19 Segall and Simpson, 1986; Fousseis et al., 2006; Pennacchioni, 2005; Pennacchioni and
20 Mancktelow, 2007). It is therefore of crucial importance to recognise the main parameters
21 controlling systems in which brittle and ductile deformation coexist. We understand brittle
22 behaviour here as deformation showing loss of cohesion along discrete surfaces, and we
23 therefore assume that it results in strongly localised systems. In a different manner, we
24 consider that ductile strain can be localised or distributed. Ductile localisation is characterised
25 by zones of localised deformation with continuous variations of strain across their width (i.e.
26 without discontinuity) and without loss of cohesion (e.g. Twiss and Moores, 1992). Fig. 1
27 shows an illustrative example of the interaction of brittle and ductile deformation in a
28 deformed quartzite (Cap de Creus, E Pyrenees, N Spain), in a greenschist environment
29 (Gomez-Rivas et al., 2007). Layers, defined by grain-size variations and preferential
30 orientation of phyllosilicates, can be used as markers to track the displacement field. They
31 show that these rocks coevally fractured and flowed, as evidenced by the presence of isoclinal
32 folds outside fracture zones and drag folds associated with small-scale faults. The resulting

1 fractures present relatively high values of maximum displacement (d_{max}) to length (L) ratios,
2 with strong gradients along them. It is a common observation that d_{max}/L ratios are
3 significantly higher in systems dominated by ductile deformation (on the order of $\sim 10^{-1}$, e.g.
4 Gomez-Rivas and Griera, 2011; Grasemann et al., 2011) than in brittle media (which range
5 from $\sim 10^{-2}$ to $\sim 10^{-4}$) (e.g. Walsh and Watterson, 1987; Kim and Sanderson, 2005). This can be
6 explained by the low propagation rate and rotation of fractures in ductile media compared to
7 those in elastic-brittle rocks.

8 The formation of brittle fractures in elastoplastic materials is a relatively well-known process
9 (e.g. Mandl, 2000 and references therein). However, there are still many open questions about
10 how fractures and shear bands form and evolve in rocks deformed by dominant viscous flow.
11 Conceptually, brittle fractures will normally develop in a ductile medium if viscous flow is
12 not able to relax the loading stress, therefore reaching the strength limit of the material. Under
13 these conditions, fracture propagation has to be studied as a time-independent process,
14 because plastic strain work at crack tips is significantly increased during propagation and can
15 result in a reduction of fracture propagation rates (e.g. Perez, 2004). A number of factors
16 determine the characteristics of the resulting fracture network in such complex coupled
17 systems (e.g. amount of fractures, formation mechanisms, orientations, type, connectivity,
18 displacement). One of these factors is material stiffness, which defines how rigid a material is,
19 and can therefore determine the relative ratio of loading rate to the rate of stress relaxation by
20 viscous flow, which at the end would control material strength in a ductile system (i.e. how
21 the rock resists deformation). Indeed, viscosity defines the rock's resistance to deformation by
22 shear and tensile stresses, and can therefore control the brittle-to-ductile transition. Another
23 relevant factor is the degree of anisotropy, which can induce a directional dependence of the
24 resistance to deform. Transverse anisotropy is a very common type of rock heterogeneity, and
25 can arise from the stacking of layers with different properties (i.e. composite anisotropy;
26 Treagus, 1997) and/or from the presence of preferentially oriented planar minerals (i.e.
27 intrinsic anisotropy; e.g. Griera et al., 2013).

28 This contribution presents an experimental study of the influence of material strength and the
29 degree and type of anisotropy on the formation of brittle fractures in ductile multilayers under
30 low effective confinement. Plasticine multilayers with different mechanical properties and
31 anisotropies have been coaxially deformed at constant strain rate, to visualise the transition
32 from non-localising systems to models where deformation is strongly localised along a few

1 large fractures. Layers in these experiments are oriented parallel to the extension direction,
2 and perpendicular to the maximum compression. We aim to address cases where effective
3 confining pressure is relatively low, like ductile rocks at shallow depths (e.g. clays, salt
4 bodies, etc.) or middle- to lower crust rocks with high fluid pressures or subjected to local
5 tensional stress (e.g. Fagereng, 2013). We aim to: (1) analyse the influence of material
6 strength on the transition from non-localising to strongly localised systems using the same
7 deformation conditions and very similar analogue materials, (2) address the role of different
8 types of transverse anisotropy (composite and composite-intrinsic) on the degree of
9 localisation and developed structures, (3) understand how coeval ductile-brittle deformation is
10 visualised in terms of stress-strain relations, and (4) capture the key factors controlling the
11 style and characteristics of the resulting structures (tension and shear fractures, pinch-and-
12 swell) and how they evolve towards well-developed fracture networks with different
13 properties (orientations, displacement-length ratios, etc.). In order to provide proper dynamic
14 scaling and define the mechanical reference framework, the rheology of the analogue
15 materials was characterised prior to experiments with uniaxial compression and relaxation
16 tests.

17

18 **2 Materials and methods**

19 **2.1 Deformation apparatus**

20 A strain rate and temperature controlled apparatus (BCN-stage; Carreras et al., 2000) was
21 used to deform the plasticine models. The prototype is based at the Universitat Autònoma de
22 Barcelona (Spain), and can apply deformations from pure to simple shear ($0 < W_k < 1$) at
23 variable temperatures. This apparatus has been used for several analogue modelling studies
24 (Druguet and Carreras, 2006; Bons et al., 2008; Druguet and Castaño, 2010; Gomez-Rivas,
25 2008; Gomez-Rivas and Griera, 2009; 2011; 2012).

26 **2.2 Experimental setup and deformation conditions**

27 Plasticine is an ideal analogue of rocks undergoing coeval ductile and brittle deformation,
28 because it can flow and also fracture at the same time depending on its composition and
29 deformation conditions (temperature, strain rate, boundary conditions). It therefore presents
30 elastoviscoplastic behaviour. Two kinds of commercial plasticine were utilised in this study.

1 They were sold under the trademarks OCLU-PLAST and JOVI, both manufactured in
2 Barcelona (Spain). Using them as a base, four different mixtures were created in order to
3 build four models: type A (white and purple OCLU-PLAST pure plasticine), type B (white
4 and purple OCLU-PLAST plasticine mixed with 10% paper flakes), type C (white and green
5 JOVI pure plasticine) and type D (blue and red JOVI plasticine mixed with 10% paper
6 flakes). Please note that the type A plasticine was the same material used for the experiments
7 of Gomez-Rivas and Griera (2011; 2012). Flakes were made of different coloured paper and
8 had a size of $\sim 2\text{mm}$ and a density of 80gr/m^2 . The models were created by stacking layers (4
9 to 5 mm thick) of alternating colours, oriented perpendicular to the Z-direction (Fig. 2).
10 Materials were mixed by hand at room temperature, and then flattened with an industrial
11 rolling pin. In that way, paper flakes were preferentially oriented parallel to layers. This
12 procedure also avoided the presence of air bubbles within the models.

13 Transverse anisotropy in all models was defined by the stacking of beds, which created a
14 composite layering. Additionally, experiments containing paper flakes (B and D) also
15 presented an intrinsic anisotropy defined by their preferred orientation. Each model had an
16 initial size of $30 \times 15 \times 10$ cm, and was compressed in the Z-direction and extended in the X-
17 direction, while the Y-direction remained constant using a reinforced transparent glass. Strain
18 rate and temperature were kept constant at $2 \times 10^{-5} \text{ s}^{-1}$ and $26 \text{ }^\circ\text{C}$, respectively. The samples
19 were deformed until a bulk finite strain ratio of $RX/Z \sim 4$ (i.e. $\sim 50\%$ shortening). Stress was
20 recorded using gauges parallel to X and Z. Digital pictures of the upper surface (X-Z plane)
21 were taken every 1% shortening. Frictional effects were minimised by lubricating the press
22 boundaries with vaseline, as well as the top surface with glycerine. Each model was biaxially
23 compressed during 24 hours at ~ 10 kPa prior to deformation, in order to bond layers and
24 avoid further interlayer slipping.

25 A 100-cm^2 area at the centre of each model was used for acquiring fracture data and
26 observations, thus avoiding boundary effects such as friction with walls. The following
27 parameters were systematically measured on all fractures at 10% shortening intervals: fracture
28 length (L), angle between fracture and the Z-axis (δ) and cumulative fracture displacement
29 (d_{max}). In order to minimise personal bias effects while collecting data, both authors
30 independently acquired measurements and the root mean square deviation normalised to mean
31 values was systematically calculated for each parameter.

1 The degree of localisation was macroscopically estimated with a strain localisation factor
2 (I_{loc}). We defined this parameter as the ratio of the maximum to the minimum shortening
3 measured using reference layers for each model (see section 3), which were used as normal
4 shortening markers. Homogeneous deformation would result in $I_{loc}=1$.

5 **2.3 Mechanical properties of the experimental materials**

6 Prior to carrying out the experiments, the mechanical properties of each analogue material
7 were characterised with uniaxial compression and relaxation tests at variable strain rates and
8 temperatures. A total of 30 tests were performed by deforming 10 cm cubes up to a minimum
9 20% shortening at variable strain rates, using the same deformation apparatus and procedure
10 as for the final experiments. The methods and equations for these tests are described in detail
11 in Gomez-Rivas and Griera (2011), and are based on the studies of McClay (1976),
12 Weijermars and Schmeling (1986), Mancktelow (1988), Ranalli (1995), Schopfer and Zulauf
13 (2002) and Zulauf and Zulauf (2004).

14 The conditions at which the tests were run, and the parameters resulting from them are
15 summarised in Tables 1 and 2 and Figs. 3 and 4. It is important to notice that the samples did
16 not fracture during uniaxial compression. The results indicate that these mixtures behave as
17 non-linear elastoviscous materials with stress exponents ranging from $n\sim 3-4$ for pure
18 plasticine (types A and C) to $n\sim 4.5-5$ for mixtures containing plasticine and paper flakes
19 (types B and D). The correlation coefficients (R^2) calculated from the log diagrams of strain
20 rate vs. stress range between 0.73 and 0.98. A marked strain hardening can be identified from
21 strain-stress curves for most of the tests (Fig. 3). Clear yield stresses can be detected in most
22 of the tests made of OCLU-PLAST and in some made of JOVI plasticine. However, not all
23 tests present yield stress, especially those with a higher viscoelastic response (Fig. 3f). The
24 viscosities of the mixtures made of JOVI plasticine (C, D) are considerably higher than the
25 ones composed of OCLU-PLAST (A, B). Adding paper flakes to plasticine makes the
26 material stiffer and increases the non-linearity behaviour of the mixture. The addition of dye
27 (purple or green) to plasticine makes it slightly softer and more non-linear than the white one,
28 although its rheology does not significantly change. Strain vs. effective viscosity curves
29 reveal a marked strain-rate softening (Fig. 4). These two types of plasticine have an effective
30 viscosity between $\sim 0.6 \times 10^9$ and $\sim 3 \times 10^9$ Pa s at low strain rates, and thus behave in a similar
31 way than other kinds of plasticine used by other authors (see Fig. 4, references included in the
32 figure).

1 Relaxation tests (i.e. stress evolution under constant strain) revealed that the estimated elastic
2 shear modulus (G) ranges between 2.4×10^6 and 4.3×10^6 Pa for mixtures made of the softer
3 plasticine (types A and B), and between 8.1×10^6 and 1.2×10^7 Pa for mixtures made of the
4 harder plasticine (types C and D) (Table 2). The Deborah number (De) (Reiner, 1964) is a
5 non-dimensional factor that defines how fluid a material is, and it is equivalent to the ratio of
6 the time of relaxation (Maxwell time, τ_m) and the time of observation (strain rate, $\dot{\epsilon}$).
7 Estimated De values (between 3.8×10^{-3} and 5.8×10^{-3} ; Table 2) indicate that our
8 experimental materials have the typical relaxation behaviour of a viscoelastic solid (e.g.
9 Poliakov et al, 1993).

10 Models A and C have a relative low degree of anisotropy because of the low viscosity
11 contrast between alternating layers. On the contrary, models B and D are significantly more
12 anisotropic, since they contain preferentially oriented paper flakes. Gomez-Rivas and Grier
13 (2009) estimated a degree of anisotropy of ~ 6 for experiments that used a very similar
14 composition to type B.

15 **2.4 Model scaling**

16 The experiments presented in this study are scaled based on the geometrical and dynamic
17 similarity of the observed deformation. Since we address fracture formation at the mesoscale,
18 we can consider a ratio of 1:1 between the experimental and natural scales in space. Viscosity
19 and strain rate values of experimental and natural materials are presented in Table 3 for their
20 dynamic scaling. If we assume a natural strain rate of the order of 10^{-14} s^{-1} (Pfiffner and
21 Ramsay, 1982), then one experimental second (at $\dot{\epsilon} = 2 \times 10^{-5} \text{ s}^{-1}$) is approximately equivalent
22 to ~ 60 natural years. In such a case, the equivalent maximum and minimum natural viscosities
23 would correspond to $\sim 2 \times 10^{18} \text{ Pa}\cdot\text{s}$ for the type A mixture and $\sim 10^{19} \text{ Pa}\cdot\text{s}$ for the type D
24 mixture, respectively. These values of scaled viscosities are of a similar order than the
25 estimated ones for schists in the middle crust ($\sim 10^{19} \text{ Pa}\cdot\text{s}$, Davidson et al., 1994) (Table 3).

26

27 **3 Experimental results**

28 The results of the four multilayer experiments indicate that the mechanical behaviour and the
29 resulting deformation pattern are notably different depending on the material used (Fig. 5).
30 There is a marked transition from a model in which deformation is almost homogeneously

1 distributed (type A) to a system controlled by a few large fractures (type D). At the end of the
2 experiments (~50% bulk shortening), model A accommodated deformation mainly by
3 homogeneous flattening. Increasing the material strength resulted in a larger number of
4 macroscopic fractures (models B, C and D), although the characteristics of the resulting
5 fracture networks strongly varied between these three experiments. The stress-strain curves
6 (Fig. 6) reveal that recorded stresses increased systematically from model A to model D.
7 Deformation was mainly accommodated by homogeneous flow during the first deformation
8 stages in all models. Such flow was associated with a stress increase. At about 10%
9 shortening the yield stress was reached for the stiffer models (C and D), and progressively
10 decreased in these experiments up to the end without reaching a clear steady state. The first
11 macroscopic fractures were not visible until ~15%-18% shortening. In the softer models (A
12 and B) a sharp yield stress was not identified, and stress progressively rose with strain until a
13 steady state was reached. This steady state behaved slightly different in each experiment, as
14 stress kept slowly growing in model B while it slightly decreased in model A.

15 The type of fractures and their orientations with respect to the deformation axes are also
16 significantly different depending on the material (Figs. 7, 8, 9). Strain localisation and
17 material embrittlement are enhanced when stiffness (or viscosity) is increased, and therefore
18 the density and type of developed fractures strongly depend on how stiff the analogue
19 material is. After 50% bulk shortening, deformation in experiment A was mainly
20 accommodated by homogeneous flattening associated with viscous flow (Figs. 5, 8a-c). The
21 estimated strain localisation factor was $I_{loc} \sim 1.04$ and normal shortening measured using the
22 reference layers of Fig. 5 ranged between 50 and 52%. Traction structures along layer
23 interfaces associated with potential inter-layer slipping were not observed. Layers were
24 thinned with increasing deformation, and only a very small number of tension cracks and
25 shear fractures could develop in this experiment. Such structures only started to be
26 macroscopically visible after 30% - 40% shortening. Tension cracks were formed until ~40%
27 shortening. The collapse of voids and cracks gave rise to the formation of hybrid fractures (or
28 mixed mode I-II fractures). They evolved to become shear fractures organised in two
29 conjugate sets (Fig. 8a-c). With very few exceptions, shear fractures formed at angles of ~40°
30 to ~50° with respect to Z, and tended to rotate towards X at a rate significantly slower than a
31 passive line (Fig. 7a, Table 4). At the end of the experiment, the length of fractures within the
32 sampling area varied between 0.33 and 1.47 cm, following an exponential distribution. The

1 cumulative fracture slip was always less than 20% of the fracture length. Relatively variable
2 maximum displacement (d_{max}) - length (L) ratios could be found in this case (Fig. 9a).

3 The behaviour of model B, which was made of a mixture of soft plasticine and paper flakes,
4 was significantly different. The presence of heterogeneities associated with flakes enhanced
5 the nucleation of a large population of small-scale shear fractures (Fig. 5). Small voids and
6 tension cracks were also recognisable within the sample (Fig. 8d-f), although flakes prevented
7 their propagation in a way that large cracks could not form. In this case, a large number of
8 millimetre-scale voids formed at the interfaces between layers or between flakes and
9 plasticine. Pinch-and-swell and boudinage structures also started to develop in the first
10 deformation stages. Two symmetrical sets of conjugate shear fractures formed in three
11 different ways with increasing strain: (1) they directly nucleated (i.e. without precursors)
12 enhanced by the heterogeneity of the two-phase (plasticine-paper flakes) system, (2) by
13 progressive necking of pinch-and-swell and boudinage structures and (3) by coalescence and
14 collapse of voids and tension cracks (Fig. 8d-f). Shear fractures formed at an angle higher
15 than 45° with regard to the Z -axis (Fig. 7b). The percentage of fractures oriented at more than
16 45° with Z ranged between 88% at 20% shortening to more than 94% for 30%-50%
17 shortening, thus indicating that fractures slightly rotated towards X . Average orientations
18 increased between $\sim 49^\circ$ and $\sim 56^\circ$ at 20% and 50% shortening, respectively (Table 4). At the
19 end of the experiment, shear fracture lengths ranged between 0.5 and 1.9 cm. and the
20 cumulative fracture slip was approximately 25% of the total length. The ratio between
21 maximum displacement (d_{max}) and length (L) was considerable higher than that of model A
22 (Fig. 9), even though fracture propagation was not very high in model B since new fractures
23 nucleated all the time until the end of the experiment (see n values in Table 4). At the model
24 scale deformation was approximately homogeneously distributed, as evidenced by a strain
25 localisation factor of $I_{loc} \sim 1.16$ and shortening normal to the reference layers ranged between
26 47 and 54%.

27 The evolution of model C resembles that of model A, but with a considerably higher amount
28 of fractures. In this case, strain localisation was related to the nucleation and growth of a very
29 large population of relatively long tension cracks, which evolved to form two conjugate sets
30 of shear fractures with increasing strain (Fig. 7c, Table 4). Tension cracks formed during the
31 first experiment stages and up to $\sim 30\%$ shortening. When deformation increased, their
32 nucleation and propagation was aborted and they started to quickly collapse and rotate

1 towards the extension direction, thus enhancing the formation of two conjugate sets of shear
2 fractures. This process took place by void and crack collapse and coalescence and by fracture
3 segment linkage (Fig. 8g,i). Such mechanisms enhanced fracture connectivity, thus
4 amplifying the direct nucleation of secondary shear fractures. Fracture statistics illustrate the
5 clear transition from a tension- to a shear fracture-dominated system with progressive
6 deformation. Almost no shear fractures were observed at 20% shortening, while many tension
7 cracks developed. At 30% shortening there were still more tension than shear fractures, which
8 were oriented at an average of $\sim 35^\circ$ with respect to Z (with a standard deviation of $\sim 7^\circ$; Table
9 4). A marked change in the properties of the fracture network took place between 30% and
10 40% shortening. At 40% shortening only a few tension cracks remained active, while a dense
11 network of shear fractures was observed. Such fractures had at this stage widely variable
12 orientations with respect to Z (from $\sim 25^\circ$ to $\sim 55^\circ$), being 43% of them oriented at angles
13 higher than 45° . These variable orientations remained at 50% shortening, when all tension
14 cracks have disappeared. At this stage 67% of shear fractures were oriented at more than 45°
15 with Z . Despite the differences in material behaviour and type of fractures, the ratio between
16 fracture length and accumulated displacement was similar to the one observed for the type B
17 model (Fig. 9). At the model scale, strain localisation by the fracture network was resolved at
18 a length scale smaller than the sample length. The calculated normal shortening ranged
19 between 45 and 55%, and the strain localisation factor was therefore relatively low ($I_{loc} \sim 1.2$).

20 Finally, the stiffer model (type D) experienced a very different deformation history than the
21 previous three experiments. Despite this, it presents some similarities with model B, mainly
22 associated with the presence of a second phase (i.e. paper flakes). Large tension cracks were
23 not observed in model D (Fig. 5). Instead, a small number of very large shear fractures
24 developed, with lengths ranging between 2.5 and 9 cm. It is important to notice that these
25 measurements refer to individual fracture segments, but fracture zones composed of several
26 segments were of course significantly longer than that. Some of them propagated up to the
27 limits of the model and were able to accommodate considerably larger displacements than the
28 ones registered in the other three experiments (Fig. 9). This observation is clearly supported
29 by the fact that the maximum fracture displacement was approximately 40% of the total
30 fracture length. Another special feature of this model is that the two conjugate shear fracture
31 sets were not symmetric, since the sinistral set nucleated earlier than the dextral one, which
32 subsequently cross-cut and displaced the early sinistral fractures (Fig. 8j-l). Shear fractures in

1 this model were, on average, oriented at 43 to 50° with Z . However, these angles were very
2 variable and some large fractures formed a lower angle with the maximum compression axis.
3 Fractures in this model tended to accommodate deformation by slip, instead of rotating
4 towards X (Fig. 7d, Table 4), in a contrary way to the other three experiments where the two
5 sets were always symmetrical with respect to the X and Z axes. At the model scale,
6 deformation was heterogeneously distributed and strong necking was observable at the central
7 part of the experiment, where relative large shear fault zones crosscut. A strong strain
8 partitioning was detected between high and low strain domains, where layer-normal
9 shortening was about 63% and 30-36%, respectively. The strain localisation factor (I_{loc}) was
10 higher than 2.0.

11

12 **4 Discussion**

13 The experimental results obtained in this study indicate that the mechanical properties of an
14 elastoviscoplastic material have a strong influence on the degree of brittle deformation and
15 how deformation is accommodated by a fracture network (Figs. 5, 8). The style of developed
16 structures and their properties strongly depend on the material mechanical behaviour (Figs. 7,
17 9, Table 4). A marked transition from distributed to strongly localised systems can be
18 observed when variants of the same materials are deformed under the same conditions. Our
19 experiments are made on two commercial types of plasticine (OCLU-PLAST and JOVI),
20 which have a similar stress exponent when they are not mixed with other components (Table
21 1). The effective viscosity of pure JOVI plasticine is about 3 times higher than that of pure
22 OCLU-PLAST, while elastic shear modulus (G) values of mixtures made of JOVI plasticine
23 are between 2 and 6 times higher than those made of OCLU-PLAST (Table 2). These
24 variations are already high enough to result in two very different deformation systems, since
25 model A (made of pure OCLU-PLAST plasticine) mostly accommodated deformation by
26 homogeneous flattening associated with viscous flow while a dense network of tension and
27 shear fractures coeval with ductile flow developed in model C (made of pure JOVI
28 plasticine). The stronger elastoviscous behaviour of type C plasticine does not allow an
29 efficient stress relaxation by viscous flow, even for high deformation values ($> 25\%$
30 shortening), thus enhancing fracture formation. The addition of paper flakes as a second
31 phase, statistically oriented parallel to layering, produced again a remarkably different
32 mechanical behaviour. A dense network of small shear fractures formed in model B (made of

1 OCLU-PLAST plasticine and flakes), while a few large fractures controlling the system
2 developed in the most rigid experiment (model D, made of JOVI plasticine and paper flakes).

3 As explained in section 2.3, no shear bands or fractures formed in the uniaxial compression
4 tests. This is evidenced by the lack of material discontinuities and the absence of pronounced
5 and sharp yield points in the stress-strain curves (Fig. 3). This does not only apply to tests
6 made of pure plasticine, but also to tests composed of mixtures B and D, which include paper
7 flakes randomly oriented. These observations suggest that the presence of heterogeneities
8 within the material is required to produce fracture onset. In our experiments, heterogeneities
9 are associated with two types of transverse anisotropy: (1) composite anisotropy (Treagus,
10 1997) defined by stacking of layers with slight contrasting properties and (2) intrinsic
11 anisotropy produced by the preferred orientation of elements of a second phase (i.e. paper
12 flakes) statistically oriented parallel to layering. All experiments are composites, but models
13 B and D include an additional intrinsic anisotropy. The type and degree of anisotropy
14 (composite *vs.* intrinsic) can play a fundamental role on the resulting structures and the bulk
15 material behaviour (Griera et al., 2011; 2013). Apart from the presence of heterogeneities,
16 another reason why brittle structures nucleate could be tectonic underpressure produced by
17 weak interfaces or contrasting rheologies between adjacent layers (e.g. Mancktelow, 2008b).
18 However, all structures in our models (voids and tension cracks, shear fractures, pinch-and-
19 swell, necking and boudinage) affect ~~both~~ all layers of different colours in the same way. This
20 indicates that tectonic underpressure is not the reason why brittle behaviour becomes active in
21 these experiments, since the competence contrast between alternating layers is very low and
22 layers are well bonded thus defining strong interfaces.

23 The transition from ductile to coeval ductile-brittle behaviour is determined by the ability of
24 the material to dissipate the imposed external work and relax the elastic strain energy stored
25 as a consequence of loading (e.g. Anderson, 2005). This relaxation can take place either by
26 viscous or coeval viscous-brittle deformation. New fractures can only grow when the strain
27 energy released during fracture growth exceeds the sum of the surface energy of the new
28 crack segment and the plastic deformation energy at the crack tip (e.g. Perez, 2004). These
29 processes strongly depend on the material strength. Stress-strain curves are used to establish a
30 qualitative relationship between the strain localisation pattern and the work necessary to
31 deform the sample. Such curves reveal a higher degree of localisation in the harder model
32 (type D), which registered a marked strain softening behaviour following the stress peak

1 (~12% shortening) (Fig. 6). The localisation of fracture networks is related to a reduction of
2 the active volume that is being deformed and an increase on the efficiency of the
3 accommodation of the imposed shortening by fracture slip. The growth of a network of few
4 large fractures in the most viscous model (type D), or the development of a well arranged but
5 segmented fracture network in experiment C, results in strain softening after yielding (Figs. 5,
6 6). Fracture networks in these two models were able to accommodate the displacement
7 imposed by the boundary conditions, although experiment C also deformed coevally by
8 dominant viscous flow. Model A basically deformed by viscous flow, and the resulting stress-
9 strain curve displays first a slight increase, and then a steady-state flow with gentle strain
10 softening after ~25% shortening. On the contrary, model B evolved by coeval small-scale
11 fracturing and viscous flow. Deformation was distributed in a large population of small shear
12 fractures with low propagation rates. Viscous relaxation was able to soften the increase of
13 stress and inhibit the propagation of large faults in this case, and the stress-strain curve thus
14 registered a very slight hardening associated with steady-state flow.

15 When loading started, ductile deformation was dominant in all models and macroscopic
16 fractures only began to nucleate after 15-20% shortening. The type of early structures strongly
17 depends on whether the anisotropy is only composite (modes A and C) or composite plus
18 intrinsic (models B and D). In composite anisotropic experiments, the first developed
19 fractures were relatively large tension cracks that evolved to mixed-mode and shear fractures
20 when fault planes rotated towards the extensional direction or when cracks collapsed and
21 coalesced (Figs. 7, 8a-c). Shear fractures in these cases are oriented at ~45° with regard to the
22 maximum compression axis Z . On the contrary, the presence of **hard flakes** prevented the
23 propagation of large tensional cracks in composite-intrinsic experiments, but enhanced the
24 nucleation of numerous small voids. Their fast collapse favours the formation of a conjugate
25 shear fracture network oriented at relative high angles from the maximum compressive stress.
26 Very small cracks and voids were visible in model B but they were not the only precursors of
27 shear fractures, since the latter could also nucleate directly from heterogeneities associated
28 with the presence of flakes. Not many tension cracks were observed in model D, suggesting
29 that this material accumulated stresses until brittle yielding was reached and then relatively
30 large shear fractures directly nucleated. Tension cracks are related to low effective confining
31 pressure and low differential stress conditions, which enhance the presence of tensional
32 stresses. Such cracks stop nucleating when viscous flow and/or slip along the shear fracture

1 network are more efficient in dissipating the applied stress. Gomez-Rivas and Griera (2011)
2 presented experiments with the model A configuration, but performed at different strain rates,
3 and found that tension cracks can form until the end of the experiment if the strain rate is high
4 enough (10^{-4} s^{-1}). This is an indication that the strain rate at which we performed our
5 experiments allows a transition from extensional- to shear fracture-dominated systems with
6 progressive deformation.

7 The collapse and coalescence of tension cracks and voids formed as a result of local layer-
8 perpendicular extension or by cavitation processes (Bons et al., 2004; 2008; 2010; Arslan et
9 al., 2008; Rybacki et al., 2008; Fousseis et al., 2009) can result in the development of shear
10 fractures in mid and lower crust rocks. Fig. 8 illustrates how shear fractures form as a
11 consequence of a single void collapse (structures 1 and 5), rotation of a single tension crack
12 (structures 2 and 9), coalescence and linkage of several cracks or voids (structures 11 and 12),
13 direct nucleation from small-scale heterogeneities (structures 6, 14 and 15) or linkage of pre-
14 existing mixed-mode or shear fractures (structures 7, 8, 10, 12, 14 and 15). The variety of
15 fracture formation mechanisms indicates that caution has to be taken when using failure
16 criteria to predict fracture formation in ductile and anisotropic rocks. However, in spite of the
17 complex localisation mechanisms, most shear fractures form at orientations close to 45° with
18 regard to Z , as predicted by the Tresca criterion (e.g. Twiss and Moores, 1992) in models A, C
19 and D. This implies that shear fractures develop in the same orientation ~~than~~ the maximum
20 shear stress, ~~evidencing~~ a very low frictional behaviour of plasticine. However, when intrinsic
21 anisotropy is present and the material is relatively soft (i.e. model B), shear fractures form at
22 an angle higher than 45° with Z . This phenomenon has been observed in a variety of field and
23 experimental studies, where the principal compressive stress σ_1 is parallel to the obtuse
24 bisector between conjugate shear band or shear fracture sets (e.g. Cobbold et al., 1971; Platt
25 and Vissers, 1980; Berhmann, 1987; Harris and Cobbold, 1984; Hanmer et al., 1996; Kidan
26 and Cosgrove, 1996; Mancktelow and Pennacchioni, 2005; Gomez-Rivas et al., 2007;
27 Pennacchioni and Mancktelow, 2007; Gomez-Rivas and Griera, 2012). Such large angles can
28 be related to a variety of factors, including fracture rotation towards the extension direction,
29 re-activation of pre-existing structures (especially when they are frictionally weak surfaces),
30 cataclastic grain size reduction or pressure-driven processes. Since some of these processes do
31 not operate in our models, we consider that the high dihedral angles in our experiment B are
32 associated with the almost absent frictional behaviour of plasticine (e.g. MacClay, 1976;
33 Zulauf and Zulauf, 2004) combined with low fracture propagation due to dominant viscous

1 flow and presence of planar heterogeneities (as in the experiments presented in Gomez-Rivas
2 and Griera, 2012).

3 **As evidenced** by average fracture lengths (L) and number of fractures per set (n) in Table 4,
4 fracture propagation and connectivity are low in models A, B and C, while they are relatively
5 higher in model D. Both conjugate sets of shear fractures have similar lengths, displacements
6 and a symmetric arrangement with respect to the compression axis in experiments A, B and C
7 (Figs. 5, 7, 9). This is coherent with the imposed coaxial deformation conditions and a
8 symmetrical orientation of layers with regard to the principal stress axes Z and X . In these
9 experiments large fractures crosscutting the entire model did not develop. Although stresses
10 were high enough to activate the onset of brittle tensile and shear fractures, the high material
11 toughness reduced the ability of fractures to propagate, making it easier for them to grow by
12 linkage and dissipate imposed stresses by nucleation of new fractures rather than propagating
13 existing ones. On the contrary, the stiffer experiment (model D) did not display a symmetric
14 distribution of both sets of fractures. In such case the dextral shear sense array is predominant
15 over the sinistral one, despite the coaxial boundary conditions and the initial orientation of
16 layers parallel to X . A strong strain partitioning between low and high strain bands can be
17 observed in this model. Large fracture zones crosscutting the model dominate deformation in
18 this experiment. They accommodate the imposed deformation and prevent the growth of a
19 small-scale conjugate shear fracture network. The formation of large fractures controlling the
20 system is related to a release of the stored elastic energy during crack growth (e.g. Perez,
21 2004) and an associated increase of their growth rate. This can be explained by the higher
22 stiffness and viscoelastic behaviour of the material that require longer times to relax elastic
23 stresses by viscous flow. The large stored elastic energy during the shear fractures onset is
24 probably the driving force that can explain the relative higher fracture propagation rates in
25 this experiment, and therefore the associated development of a few long fractures.

26 Experimental observations evidence that fracture growth is a consequence of a combination of
27 fault tip propagation with slip increase and segmentation linkage (Walsh et al., 2002). The
28 strength of the deforming material partially controls the ratio between the maximum
29 displacement of each fault (d_{max}) and its length (L). The relationship between these two
30 parameters depends on the fault displacement, expressed in the parameter c , and an exponent
31 m (Kim and Sanderson, 2005):

$$32 \quad d_{max} = cL^m \quad (1)$$

1 This relationship in our models is approximately linear in a log-log graph, although the
2 limited data range prevents extrapolating these data to larger scales. The d_{max}/L ratios
3 observed in this series of experiments range between 0.12 and 0.23 (Fig. 9), and are therefore
4 higher than the ones inferred from natural faults, which vary between $\sim 10^{-1}$ and $\sim 10^{-2}$; e.g.
5 Kim and Sanderson, 2005). There is a progressive increase in the d_{max}/L ratio when the
6 material strength is raised, systematically from model A (softer) to model D (tougher).
7 Gomez-Rivas and Griera (2011) also reported that strain rate increases the
8 displacement/length relationship. Such relationships in our experiments are considerably
9 higher than in other cases previously reported in the literature (e.g. Kim and Sanderson, 2005
10 and references therein), mostly from brittle rocks. However, Grasmann et al. (2011) found
11 similar values in small-scale fractures ~~with~~ associated flanking folds within a low-grade
12 ductile shear zone. This suggests that fault displacement-length relationships are probably
13 higher in rocks that undergo dominant ductile deformation. Since shear fractures in our
14 experiments are easy slip zones (i.e. weak-faults), a significant amount of deformation can be
15 accommodated by displacement along fractures, especially in the harder models. However,
16 the high material toughness prevents fractures ~~to propagate~~, thus resulting in relatively high
17 d_{max}/L values. Fracture propagation requires the release of a certain amount of energy at crack
18 tips, which are areas of strain hardening. The dominant viscous deformation of models A, B
19 and C does not allow enough energy accumulation at crack tips for propagation. On the
20 contrary, such energy is high enough in model D, where fractures could grow.

21 The results of the experiments presented in this study contribute to the understanding of the
22 main controls on fracture localisation in ductile materials as well as the accommodation of
23 deformation by different fracture networks depending on the rock mechanical properties.
24 These models illustrate how strain localisation processes operate in a dominant ductile regime
25 and allow visualising the transition from brittle to ductile behaviour using materials with a
26 similar rheology. The progressive onset, interaction and evolution of different types of
27 structures (tension cracks, voids, pinch-and-swell, hybrid fractures, shear fractures) define a
28 progressive change in the behaviour of the system. The presence of composite or combined
29 composite-intrinsic transverse anisotropy plays a fundamental role, since it enhances brittle
30 behaviour, promoting fracture formation and helping to dissipate the applied stress.

31

1 **5 Conclusions**

2 This contribution presents an experimental study on the influence of material strength on the
3 formation of fracture networks in materials that are deformed by dominant viscous flow. Four
4 plasticine multilayers, made of different mixtures, were deformed under coaxial boundary
5 conditions at a constant strain rate and temperature. The following main conclusions arise
6 from these experiments:

7 1. The increase of material strength causes a progressive transition from a non-localising end
8 member, where deformation is mostly accommodated by homogeneous flattening, to a
9 strongly localised system where a few fractures accommodate displacement. This ductile-to-
10 brittle transition is controlled by the ability of the material to dissipate the external work and
11 relax the elastic strain during loading, either by viscous flow or coeval flow and failure. Shear
12 fractures, which are oriented at $\sim 45^\circ$ from σ_I in most experiments, form by the collapse and
13 coalescence of tension cracks and voids, from the evolution of pinch-and-swell structures or
14 by direct nucleation associated with heterogeneities.

15 2. Stress-strain curves record the progressive transition from ductile-dominated to fracture-
16 dominated systems. Models deformed by dominant viscous flow are characterised by the
17 absence of yield points and a slight stress increase followed by steady state behaviour. On the
18 contrary, localising systems record higher stress magnitudes and clear yield points followed
19 by subsequent strain softening associated with deformation accommodated by fractures.

20 3. Additional intrinsic anisotropy, resulting from the presence paper flakes statistically
21 oriented parallel to layers, produces a change in the deformation behaviour inhibiting the
22 nucleation of tension cracks and voids. Enhanced transverse anisotropy in the soft model
23 reduces fracture propagation and favours the formation a dense network of small-scale shear
24 fractures oriented at high angles ($> 45^\circ$) with σ_I . On the contrary, flakes significantly increase
25 the rigidity of the material when added to the harder plasticine, and promote the formation of
26 an asymmetric arrangement of a reduced number of large fractures controlling the system.

27 4. Material strength increases the fracture maximum displacement (d_{max}) to length (L) ratios.
28 Such values are relatively high compared to those resulting from fractures formed in elastic-
29 brittle media. This is associated with the low propagation rates of fractures in rocks
30 undergoing ductile deformation, and also with the presence of anisotropy.

31

1 **Acknowledgements**

2 This work was financed through the research project CGL2004-03657, funded by the Spanish
3 Ministry of Education and Science. We thank J. Carreras, E. Druguet and L.M. Castaño for
4 discussions on some aspects related to this work.

5

6 **References**

- 7 Anderson, T. L.: Fracture mechanics: fundamentals and applications. Taylor and Francis.,
8 2005.
- 9 Arslan, A., Passchier, C. W., and Koehn, D.: Foliation boudinage, *J. Struct. Geol.*, 30(3),
10 291–309, 2008.
- 11 Behrmann, J. H.: A precautionary note on shear bands as kinematic indicators, *J. Struct.*
12 *Geol.*, 9(5-6), 659–IN8, 1987.
- 13 Bons, P. D., Becker, J. K., Elburg, M. A., and Urtson, K.: Granite formation: Stepwise
14 accumulation of melt or connected networks?, *Earth Environ. Sci. Trans. R. Soc. Edinburgh*,
15 100(1-2), 105–115, 2010.
- 16 Bons, P. D., Druguet, E., Castaño, L.-M., and Elburg, M. A.: Finding what is now not there
17 anymore: Recognizing missing fluid and magma volumes, *Geology*, 36(11), 851, 2008.
- 18 Bons, P. D., Druguet, E., Hamann, I., Carreras, J., and Passchier, C. W.: Apparent boudinage
19 in dykes, *J. Struct. Geol.*, 26(4), 2004.
- 20 Carreras, J., Julivert, M., Soldevila, A., Griera, A., and Soler, D.: A deformation stage for
21 analogue modelling of structures developed under variable degree of non-coaxiality, in:
22 *Geoscience 2000 Abstracts volume*, University of Manchester, section *Modelling in*
23 *Structural Geology*, 126., 2000.
- 24 Cobbold, P. R., Cosgrove, J. W., and Summers, J. M.: Development of internal structures in
25 deformed anisotropic rocks, *Tectonophysics*, 12, 23–53, 1971.
- 26 Davidson, C., Schmid, S. M., and Hollister, L. S.: Role of melt during deformation in the deep
27 crust, *Terra Nov.*, 6(2), 133–142, 1994.
- 28 Druguet, E. and Carreras, J.: Analogue modelling of syntectonic leucosomes in migmatitic
29 schists, *J. Struct. Geol.*, 28(10), 1734–1747, 2006.

- 1 Druguet, E. and Castaño, L. M.: Analysis of syntectonic magmatic veins at the mesoscale, J.
2 Geol. Soc. India, 75, 60–73, 2010.
- 3 Fagereng, Å.: On stress and strain in a continuous-discontinuous shear zone undergoing
4 simple shear and volume loss, J. Struct. Geol., 50, 44–53, 2013.
- 5 Fusseis, F., Handy, M. R., and Schrank, C.: Networking of shear zones at the brittle-to-
6 viscous transition (Cap de Creus, NE Spain), J. Struct. Geol., 28(7), 1228–1243, 2006.
- 7 Fusseis, F., Regenauer-Lieb, K., Liu, J., Hough, R. M., and De Carlo, F.: Creep cavitation can
8 establish a dynamic granular fluid pump in ductile shear zones., Nature, 459(7249), 974–7,
9 2009.
- 10 Gomez-Rivas, E.: Localización de deformación en medios dúctiles y anisótopos: estudio de
11 campo, experimental y numérico. PhD thesis, Universitat Autònoma de Barcelona, 247 pp.
12 Available from: <http://www.tesisenxarxa.net/TDX-1120108-151236/>, 2008.
- 13 Gomez-Rivas, E., Bons, P. D., Griera, A., Carreras, J., Druguet, E., and Evans, L.: Strain and
14 vorticity analysis using small-scale faults and associated drag folds, J. Struct. Geol., 29(12),
15 1882–1899, 2007.
- 16 Gomez-Rivas, E. and Griera, A.: Influence of mechanical anisotropy on shear fracture
17 development, Trab. Geol., 29, 305–311, 2009.
- 18 Gomez-Rivas, E. and Griera, A.: Strain rate influence on fracture development in
19 experimental ductile multilayers, Tectonophysics, 502(3-4), 351–363, 2011.
- 20 Gomez-Rivas, E. and Griera, A.: Shear fractures in anisotropic ductile materials: an
21 experimental approach, J. Struct. Geol., 34, 61–76, 2012.
- 22 Grasemann, B., Exner, U., and Tschegg, C.: Displacement–length scaling of brittle faults in
23 ductile shear, J. Struct. Geol., 33(11), 1650–1661, 2011.
- 24 Griera, A., Bons, P. D., Jessell, M. W., Lebensohn, R. A., Evans, L., and Gomez-Rivas, E.:
25 Strain localization and porphyroclast rotation, Geology, 39(3), 275–278, 2011.
- 26 Griera, A., Llorens, M.-G., Gomez-Rivas, E., Bons, P. D., Jessell, M. W., Evans, L. A., and
27 Lebensohn, R.: Numerical modelling of porphyroclast and porphyroblast rotation in
28 anisotropic rocks, Tectonophysics, 587, 4–29, 2013.

- 1 Guermani, A., and Pennacchioni, G.: Brittle precursors of plastic deformation in a granite: an
2 example from the Mont Blanc Massif (Helvetic, Western Alps), *J. Struct. Geol.*, 20, 135-148,
3 1998.
- 4 Hanmer, S., Corrigan, D., and Ganas, A.: Orientation of nucleating faults in anisotropic
5 media: insights from three-dimensional deformation experiments, *Tectonophysics*, 267(1-4),
6 275–290, 1996.
- 7 Harris, L. B. and Cobbold, P. R.: Development of conjugate shear bands during bulk simple
8 shearing, *J. Struct. Geol.*, 7(1), 37–44, 1985.
- 9 Hobbs, B. E., Ord, A., and Teyssier, C.: Earthquakes in the ductile regime?, *Pure Appl.*
10 *Geophys.*, 124(1-2), 309–336, 1986.
- 11 Kidan, T. W. and Cosgrove, J. W.: The deformation of multilayers by layer-normal
12 compression: an experimental investigation, *J. Struct. Geol.*, 18(4), 461–474, 1996.
- 13 Kim, Y.-S. and Sanderson, D. J.: The relationship between displacement and length of faults:
14 a review, *Earth-Science Rev.*, 68(3-4), 317–334, 2005.
- 15 Mancktelow, N. S.: The rheology of paraffin wax and its usefulness as an analogue for rocks,
16 *Bull. Geol. Institutions Univ. Uppsala*, 14, 181–193, 1988.
- 17 Mancktelow, N. S.: How ductile are ductile shear zones?, *Geology*, 34(5), 345, 2006.
- 18 Mancktelow, N. S.: Interaction between brittle fracture and ductile flow during crustal
19 deformation, *Boll. della Soc. Geol. Ital.*, 127, 217–220, 2008a.
- 20 Mancktelow, N. S.: Tectonic pressure: Theoretical concepts and modelled examples, *Lithos*,
21 103(1-2), 149–177, 2008b.
- 22 Mancktelow, N. S. and Pennacchioni, G.: The control of precursor brittle fracture and fluid–
23 rock interaction on the development of single and paired ductile shear zones, *J. Struct. Geol.*,
24 27(4), 645–661, 2005.
- 25 Mancktelow, N. S.: Fracture and flow in natural rock deformation, *Trabajos de Geología*, 29,
26 29-35, 2009.
- 27 Mandl, G.: *Faulting in Brittle Rocks*, Springer-Verlag, Berlin–Heidelberg–New York., 2000.
- 28 McClay, K. R.: The rheology of plasticine, *Tectonophysics*, 33, T7–T15, 1976.

- 1 Passchier, C. W.: The generation of ductile and brittle shear bands in a low-angle mylonite
2 zone, *J. Struct. Geol.*, 6(3), 273–281, 1984.
- 3 Paterson, M. S.: *Experimental rock deformation: the brittle field*, 2nd edition, Springer-
4 Verlag, Berlin., 1978.
- 5 Pennacchioni, G., and Cesare, B.: Ductile-brittle transition in pre-Alpine amphibolite facies
6 mylonites during evolution from water-present to water-deficient conditions (Mont Mary
7 Nappe, Italian Western Alps), *J. Metamorph. Geol.*, 15, 777-791, 1997.
- 8 Pennacchioni, G.: Control of the geometry of precursor brittle structures on the type of ductile
9 shear zone in the Adamello tonalites, Southern Alps (Italy), *J. Struct. Geol.*, 27(4), 627–644,
10 2005.
- 11 Pennacchioni, G. and Mancktelow, N. S.: Nucleation and initial growth of a shear zone
12 network within compositionally and structurally heterogeneous granitoids under amphibolite
13 facies conditions, *J. Struct. Geol.*, 29(11), 1757–1780, 2007.
- 14 Perez, N.: *Fracture Mechanics*, Springer., 2004.
- 15 Pfiffner, O. and Ramsay, J.: Constraints on geological strain rates: arguments from finite
16 strain states of naturally deformed rocks, *J. Geophys. Res.-Sol. EA*, 87(B1), 311–321, 1982.
- 17 Platt, J. P. and Vissers, R. L. M.: Extensional structures in anisotropic rocks, *J. Struct. Geol.*,
18 2(4), 397–410, 1980.
- 19 Poliakov, A. N. B., Cundall, P. A., Podladchikov, Y. Y. and Lyakhovsky, V. A.: An explicit
20 inertial method for the simulation of viscoelastic flow: an evaluation of elastic effects on
21 diapiric flow in two- and three-layers models, in: *Flow and Creep in the Solar System:*
22 *Observations, Modeling and Theory*, edited by: Stone, D. B. and Runcorn, S.K., Kluwer
23 Academic Publishers, Dordrecht (Holland), 175-195, 1993.
- 24 Ranalli, G.: *Rheology of the Earth*, Chapman & Hall, London, 1995.
- 25 Reiner, M.: The Deborah Number, *Physics Today*, 17, 62, 1964.
- 26 Rybacki, E., Wirth, R., and Dresen, G.: High-strain creep of feldspar rocks: Implications for
27 cavitation and ductile failure in the lower crust, *Geophys. Res. Lett.*, 35(4), L04304, 2008.
- 28 Schöpfer, M. and Zulauf, G.: Strain-dependent rheology and the memory of plasticine,
29 *Tectonophysics*, 354, 85–99, 2002.

- 1 Segall, P. and Simpson, C.: Nucleation of ductile shear zones on dilatant fractures, *Geology*,
2 14(1), 56-59, 1986.
- 3 Simpson, C.: Deformation of granitic rocks across the brittle-ductile transition. *J. Struct.*
4 *Geol.*, 7, 503-511, 1985.
- 5 Treagus, S. H.: Deformation partitioning in folds: implications for fold geometry and
6 cleavage patterns, in: *Evolution of Geological Structures in Micro- to Macro-Scales*, edited
7 by: Sengupta, S., Chapman & Hall, London, 341–372, 1997.
- 8 Twiss, R. J. and Moores, E. M.: *Structural Geology*, W.H. Freeman, New York., 1992.
- 9 Walsh, J. J., Nicol, A. and Childs, C.: An alternative model for the growth of faults, *J. Struct.*
10 *Geol.*, 24(11), 1669–1675, 2002.
- 11 Walsh, J. J. and Watterson, J.: Distributions of cumulative displacement and seismic slip on a
12 single normal fault surface, *J. Struct. Geol.*, 9(8), 1039–1046, 1987.
- 13 Weijermars, R.: *Principles of rock mechanics*, Alboran Science Publishing, Amsterdam.,
14 1997.
- 15 Weijermars, R. and Schmeling, H.: Scaling of Newtonian and non-Newtonian fluid dynamics
16 without inertia for quantitative modelling of rock flow due to gravity (including the concept
17 of rheological similarity), *Phys. Earth Planet. Inter.*, 43, 316–330, 1986.
- 18 Zulauf, J. and Zulauf, G.: Rheology of plasticine used as rock analogue: the impact of
19 temperature, composition and strain, *J. Struct. Geol.*, 26(4), 725–737, 2004.
- 20

1 Table 1. Properties calculated from compression tests for the different mixtures used as rock
 2 analogues. The values of axial stress, dynamic effective viscosity, stress exponent and
 3 material constant were calculated for 10% shortening.

4 5 6	Type of mixture	Composition	Strain rate ($\dot{\epsilon}$) [s^{-1}]	Axial stress (σ) [Pa]	Effective viscosity (η) [Pa s]	Stress exponent (n)	Material constant (C) [$Pa^{-n} s^{-1}$]
7	A white	OCLU-PLAST white plasticine	1.8 x 10 ⁻⁵	2.4 x 10 ⁴	6.1 x 10 ⁸	3.9	1.8 x 10 ⁻²²
8			5.5 x 10 ⁻⁵	3.6 x 10 ⁴	3.0 x 10 ⁸		1.3 x 10 ⁻²²
9			1.0 x 10 ⁻⁴	3.2 x 10 ⁴	1.6 x 10 ⁸		2.7 x 10 ⁻²²
10			2.6 x 10 ⁻⁴	4.8 x 10 ⁴	4.8 x 10 ⁷		2.0 x 10 ⁻²²
11	A coloured	OCLU-PLAST coloured plasticine	1.9 x 10 ⁻⁵	2.3 x 10 ⁴	5.8 x 10 ⁸	4.1	3.5 x 10 ⁻²³
12			5.5 x 10 ⁻⁵	2.6 x 10 ⁴	2.1 x 10 ⁸		7.1 x 10 ⁻²³
13			1.0 x 10 ⁻⁴	3.8 x 10 ⁴	1.9 x 10 ⁸		1.5 x 10 ⁻²³
14			2.5 x 10 ⁻⁴	3.3 x 10 ⁴	3.3 x 10 ⁷		2.7 x 10 ⁻²²
15	B white	OCLU-PLAST white plasticine + 10% flakes	1.8 x 10 ⁻⁵	4.5 x 10 ⁴	1.1 x 10 ⁹	5.3	5.8 x 10 ⁻³⁰
17			5.4 x 10 ⁻⁵	3.6 x 10 ⁴	3.0 x 10 ⁸		4.9 x 10 ⁻²⁹
18			8.8 x 10 ⁻⁵	4.6 x 10 ⁴	2.3 x 10 ⁸		2.6 x 10 ⁻²⁹
19			2.5 x 10 ⁻⁴	4.4 x 10 ⁴	4.4 x 10 ⁷		1.9 x 10 ⁻²⁷
20	C white	JOVI white plasticine	1.9 x 10 ⁻⁵	6.9 x 10 ⁴	1.7 x 10 ⁹	3.3	2.2 x 10 ⁻²¹
22			5.5 x 10 ⁻⁵	1.0 x 10 ⁵	8.4 x 10 ⁸		2.3 x 10 ⁻²¹
23			8.9 x 10 ⁻⁵	1.0 x 10 ⁵	5.2 x 10 ⁸		3.6 x 10 ⁻²¹
24			2.1 x 10 ⁻⁴	9.3 x 10 ⁴	9.3 x 10 ⁷		4.5 x 10 ⁻¹⁹
25	C coloured	JOVI coloured plasticine	1.8 x 10 ⁻⁵	9.9 x 10 ⁴	2.5 x 10 ⁹	3.9	8.7 x 10 ⁻²⁵
27			5.3 x 10 ⁻⁵	7.5 x 10 ⁴	6.2 x 10 ⁸		8.5 x 10 ⁻²⁴
28			9.2 x 10 ⁻⁵	8.1 x 10 ⁴	4.0 x 10 ⁸		9.1 x 10 ⁻²⁴
29			2.4 x 10 ⁻⁴	1.1 x 10 ⁵	1.1 x 10 ⁸		1.0 x 10 ⁻²²
30	D white	JOVI white plasticine + 10% flakes	1.6 x 10 ⁻⁵	1.4 x 10 ⁵	3.4 x 10 ⁹	4.5	2.7 x 10 ⁻²⁸
32			5.0 x 10 ⁻⁵	8.3 x 10 ⁴	6.9 x 10 ⁸		5.9 x 10 ⁻²⁷
33			8.9 x 10 ⁻⁵	1.2 x 10 ⁵	5.8 x 10 ⁸		1.7 x 10 ⁻²⁷
34			2.4 x 10 ⁻⁴	1.2 x 10 ⁵	1.2 x 10 ⁸		7.0 x 10 ⁻²⁶
35							

36

37

1 Table 2. Summary of material properties calculated with relaxation tests for the different
 2 mixtures used as rock analogues. Only tests deformed at similar strain rates than multilayer
 3 experiments are displayed. The values of elastic shear modulus (G) and Deborah number (De)
 4 were calculated assuming a Maxwell body.

5 6	Type of mixture	Composition	Strain rate ($\dot{\epsilon}$) [s^{-1}]	Elastic shear modulus (G) [Pa]	Deborah number
7 8	A white	OCLU-PLAST white plasticine	1.8×10^{-5}	2.4×10^6	4.6×10^{-3}
9 10	A coloured	OCLU-PLAST coloured plasticine	1.9×10^{-5}	2.0×10^6	5.8×10^{-3}
11 12	B white	OCLU-PLAST white plasticine + 10% flakes	1.8×10^{-5}	4.3×10^6	4.6×10^{-3}
13 14	C white	JOVI white plasticine	1.9×10^{-5}	1.1×10^7	3.9×10^{-3}
15 16	C coloured	JOVI coloured plasticine	1.8×10^{-5}	8.1×10^6	4.8×10^{-3}
17 18	D white	JOVI white plasticine + 10% flakes	1.6×10^{-5}	1.2×10^7	3.8×10^{-3}

1 Table 3. Values of strain rate and effective viscosity of mid crustal rocks and the less and
 2 more viscous analogue materials used in this study (Types A and D mixtures, respectively).
 3 The strain rate value for mid crustal rocks was taken from Pfiffner and Ramsay (1982) and
 4 Weijermars (1997). The viscosity of schists was taken from Davidson et al. (1994).

5	Material	Strain rate ($\dot{\epsilon}$) [s^{-1}]	Deformation time	Effective viscosity η^* [$Pa \cdot s$]
6			at 50% sh. (t) [s]	
7	Mid crustal rocks	10^{-14}	$8.3 \cdot 10^{13}$ (~2.6 Ma)	$\sim 10^{18} - 10^{19}$ (schist at 500-700° C)
8	Type A mixture	$2 \cdot 10^{-5}$	$3.4 \cdot 10^4$	$6.1 \cdot 10^8$ (OCLU-PLAST plasticine)
9	Type A mixture	10^{-4}	$6.2 \cdot 10^3$	$1.6 \cdot 10^8$ (OCLU-PLAST plasticine)
10	Type D mixture	$2 \cdot 10^{-5}$	$3.4 \cdot 10^4$	$3.4 \cdot 10^9$ (JOVI plasticine + confetti)

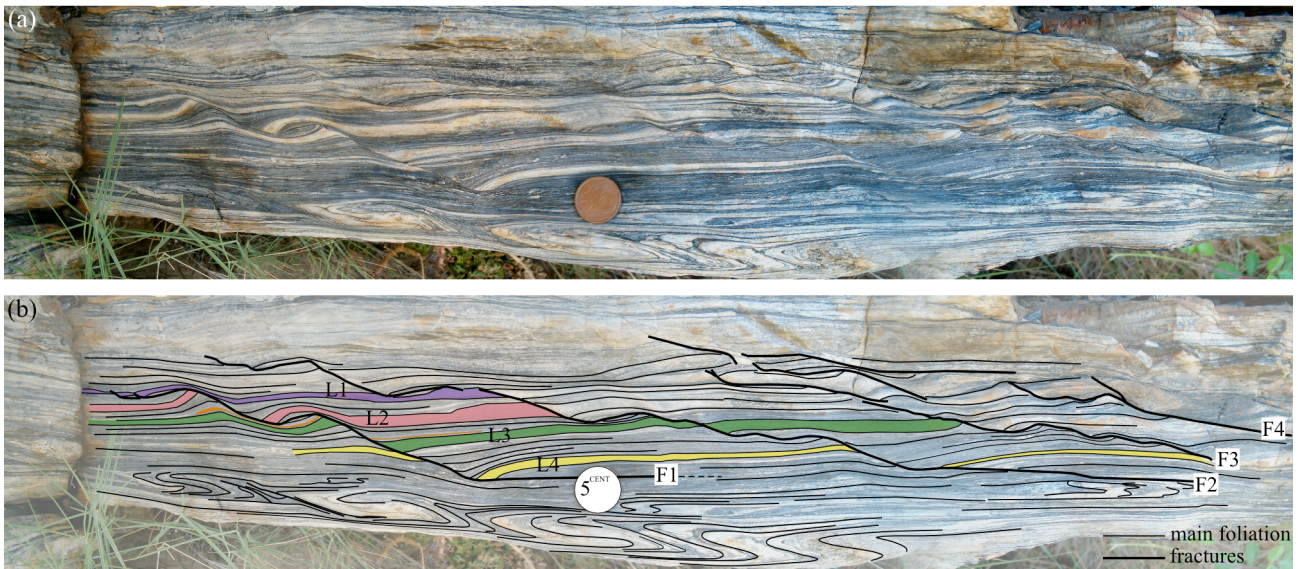
11

12

1 Table 4. Compilation of shear fracture data at shortening intervals of 20%, 30%, 40% and
2 50%. δ is the average shear fracture orientation with respect to the Z axis, measured in
3 degrees. Fracture length (L) and maximum displacement (d_{max}) of shear fractures are
4 measured in cm. Standard deviations are in parentheses. n and $n_{tension}$ indicate the total number
5 of shear fractures and tension cracks, respectively. Length (L) values do not include data from
6 tension cracks, and refer to individual fracture segments. Fault zones composed of several
7 segments are therefore longer than individual ones. The number of tension cracks for models
8 B and D is not displayed, since cracks were too small to trace them accurately. Note that data
9 corresponding to 50% shortening in model D were actually measured at 44% shortening,
10 when this experiment finished.

Experiment	Sinistral set of fractures				Dextral set of fractures			
	20%	30%	40%	50% sh.	20%	30%	40%	50% sh.
Type A								
δ	- (-)	45.3 (2.3)	47.0 (3.2)	49.1 (4.1)	- (-)	- (-)	41.1 (3.5)	48.8 (4.5)
L	- (-)	0.41 (0.17)	0.68 (0.31)	0.69 (0.33)	- (-)	- (-)	0.53 (0.10)	0.67 (0.28)
d_{max}	- (-)	0.10 (0.01)	0.11 (0.03)	0.14 (0.06)	- (-)	- (-)	0.07 (0.02)	0.12 (0.05)
n	0	2	8	12	0	0	7	14
$n_{tension}$	2	6	7	7				
Type B								
δ	48.5 (3.4)	52.0 (4.2)	53.7 (6.1)	55.4 (6.9)	49.7 (3.5)	52.3 (4.0)	55.0 (4.3)	57.6 (5.5)
L	0.67 (0.07)	0.75 (0.10)	0.77 (0.13)	0.85 (0.16)	0.71 (0.07)	0.75 (0.10)	0.85 (0.20)	0.92 (0.29)
d_{max}	0.12 (0.03)	0.14 (0.08)	0.17 (0.04)	0.22 (0.10)	0.11 (0.02)	0.13 (0.04)	0.17 (0.05)	0.22 (0.08)
n	39	63	89	136	37	71	96	132
$n_{tension}$	-	-	-	-				
Type C								
δ	21.3 (-)	31.9 (7.0)	37.0 (7.8)	42.3 (7.2)	32.3 (3.2)	36.9 (6.3)	44.6 (5.4)	49.5 (6.2)
L	0.78 (-)	0.74 (0.29)	0.79 (0.31)	0.82 (0.41)	0.56 (0.03)	0.61 (0.17)	0.78 (0.32)	0.82 (0.37)
d_{max}	0.12 (-)	0.12 (0.06)	0.15 (0.07)	0.18 (0.09)	0.07 (0.01)	0.11 (0.03)	0.19 (0.10)	0.20 (0.10)
n	1	17	41	72	3	17	40	74
$n_{tension}$	71	58	8	0				
Type D								
δ	43.8 (3.4)	43.4 (4.5)	44.0 (6.5)	44.8 (6.4)	50.2 (3.5)	45.6 (10.7)	48.4 (13.0)	48.9 (11.4)
L	0.91 (0.07)	1.16 (0.58)	1.61 (1.17)	1.74 (1.33)	1.17 (0.13)	2.35 (1.99)	2.54 (2.00)	2.56 (2.15)
d_{max}	0.27 (0.04)	0.28 (0.05)	0.46 (0.35)	0.52 (0.43)	0.28 (0.04)	0.51 (0.23)	0.63 (0.48)	0.52 (0.22)
n	4	6	14	16	6	13	16	19
$n_{tension}$	-	-	-	-				

40
41
42

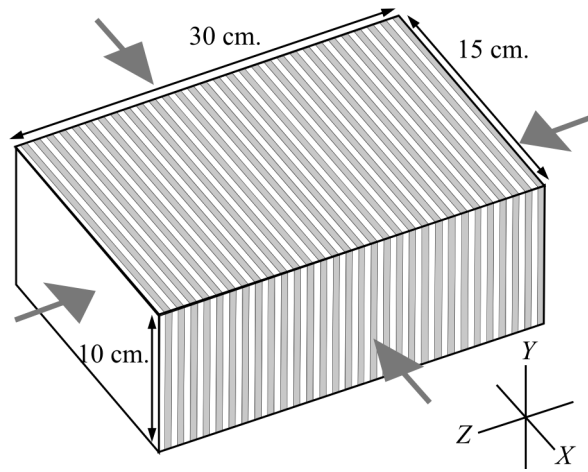


1

2

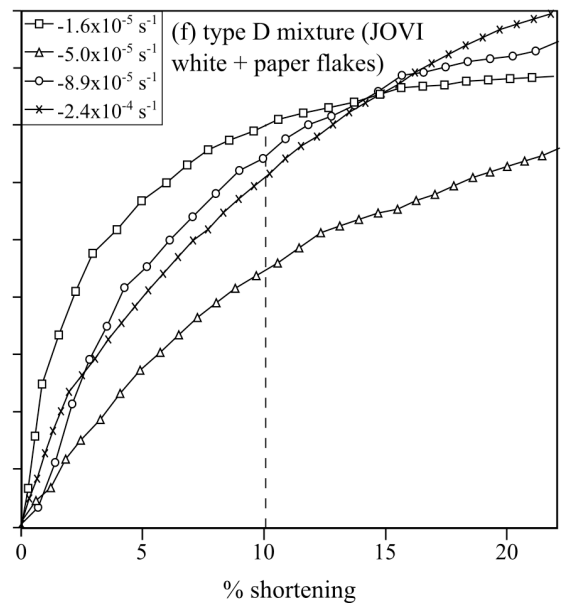
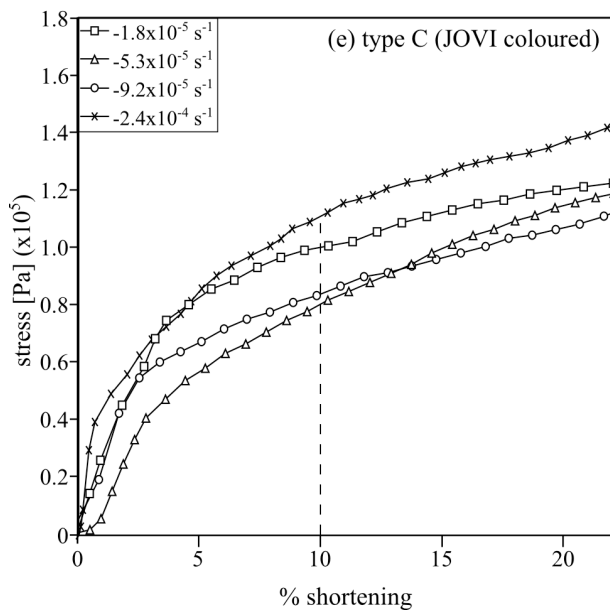
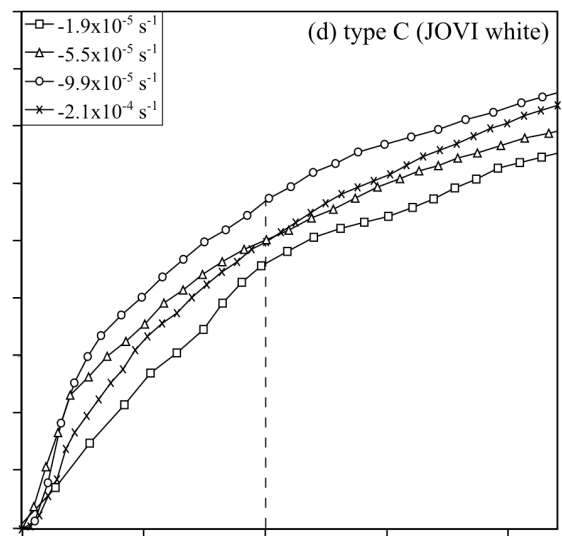
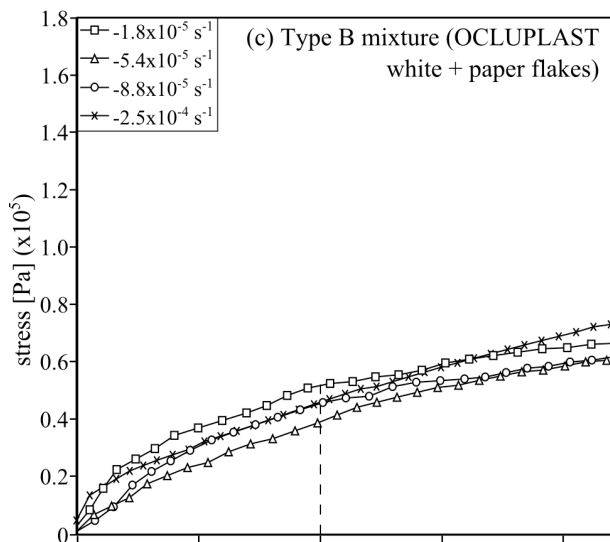
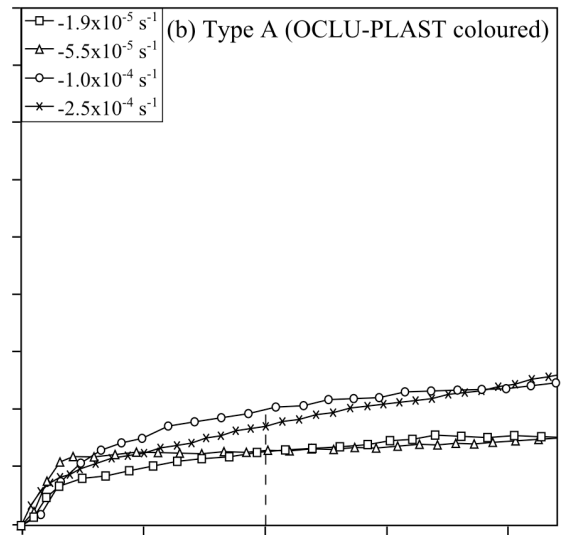
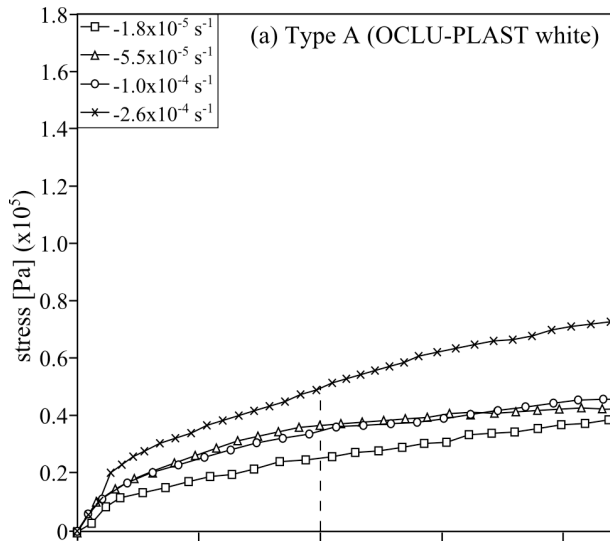
3 Figure 1. Examples of brittle deformation localisation in a ductile dominant system. (a)
 4 presents small-scale shear fractures (F1 to F4) with flat/ramp segments and roll-over
 5 geometries in deformed banded quartzites of the Rabassers outcrop, at Cap de Creus (E
 6 Pyrenees, Spain) (Gomez-Rivas et al., 2007), and (b) the interpreted structures. Fracture
 7 planes are smooth. Antithetic, synthetic and double-sense drag folds can be observed. Note
 8 that same layers at both sides of fractures do not present the same drag fold pattern.
 9 Displacements along fault surfaces are not constant and do not show an elliptical distribution,
 10 as expected for an isolated fracture. Maximum displacement – length relationships (d_{max}/L)
 11 range between 0.10 and 0.15. These fractures are interpreted as formed by segment linkage
 12 and growth during coetaneous brittle and ductile deformation. Fracture offsets of reference
 13 layers are: 0 cm (L1), 3.5-3.8 cm (L2), 2.5-3.0 cm (L3) and 3.3-3.7 cm (L4). This view is
 14 perpendicular to the foliation and fracture planes. Anisotropy of this rock is a consequence of
 15 grain size differences between dark and white layers and preferred orientation of
 16 phyllosilicates. The diameter of the 5€-cent coin is 21 mm.

17

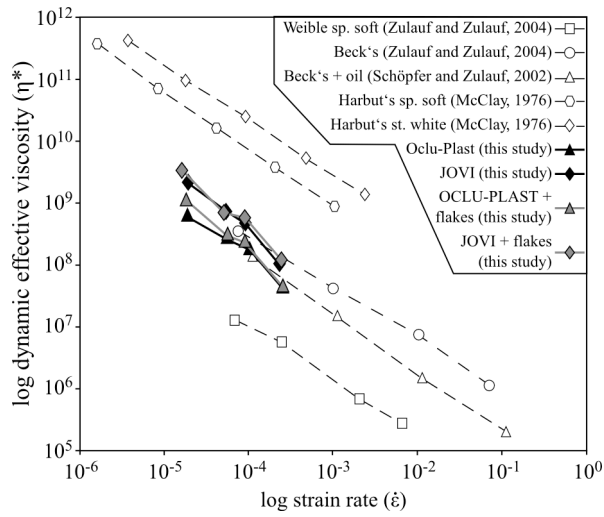


1
2
3
4
5

Figure 2. Sketch of a multilayer experiment. The arrows indicate the direction of the principal stresses applied by the deformation apparatus. The initial layer thickness was ~4-5 mm.

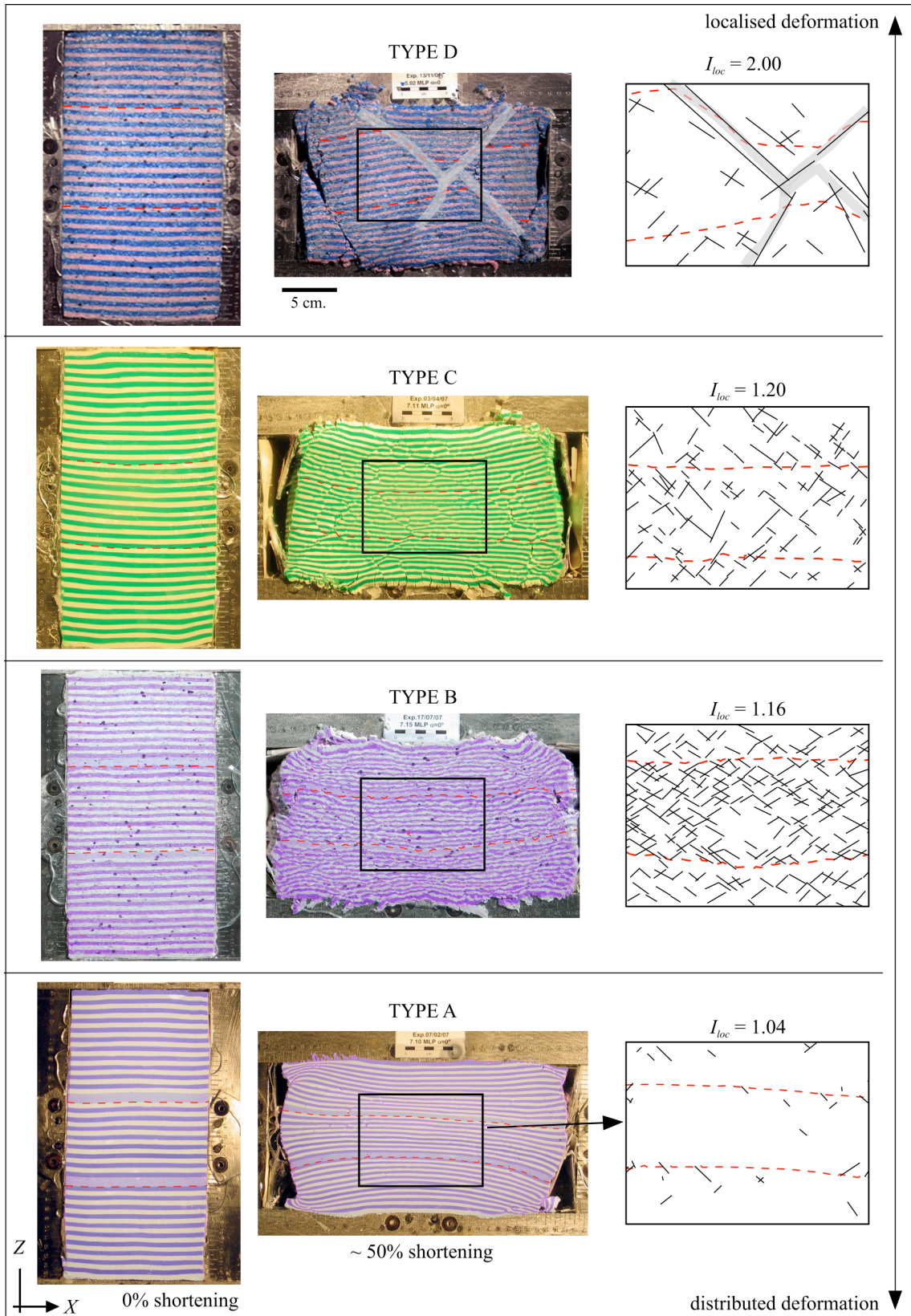


1 Figure 3. Stress vs. axial strain (expressed in % shortening) curves for the materials used in
2 this study at different strain rates. Dashed lines indicate the strain reference value used for
3 comparison of material properties (10% shortening).
4



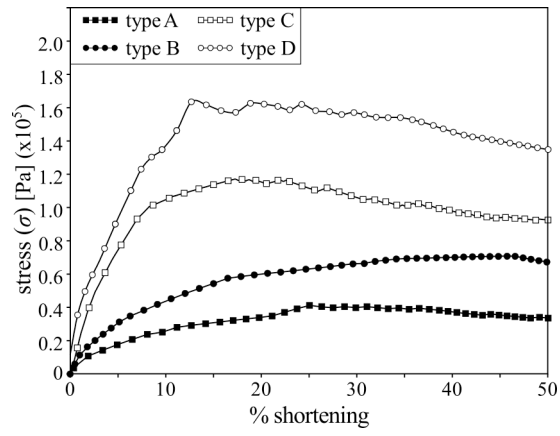
1
2
3
4
5
6

Figure 4. Log plot strain rate vs. effective dynamic viscosity comparing the mixtures used in this study with other kinds of commercially available plasticine used by other authors. Effective dynamic viscosity values were taken at 10% shortening.



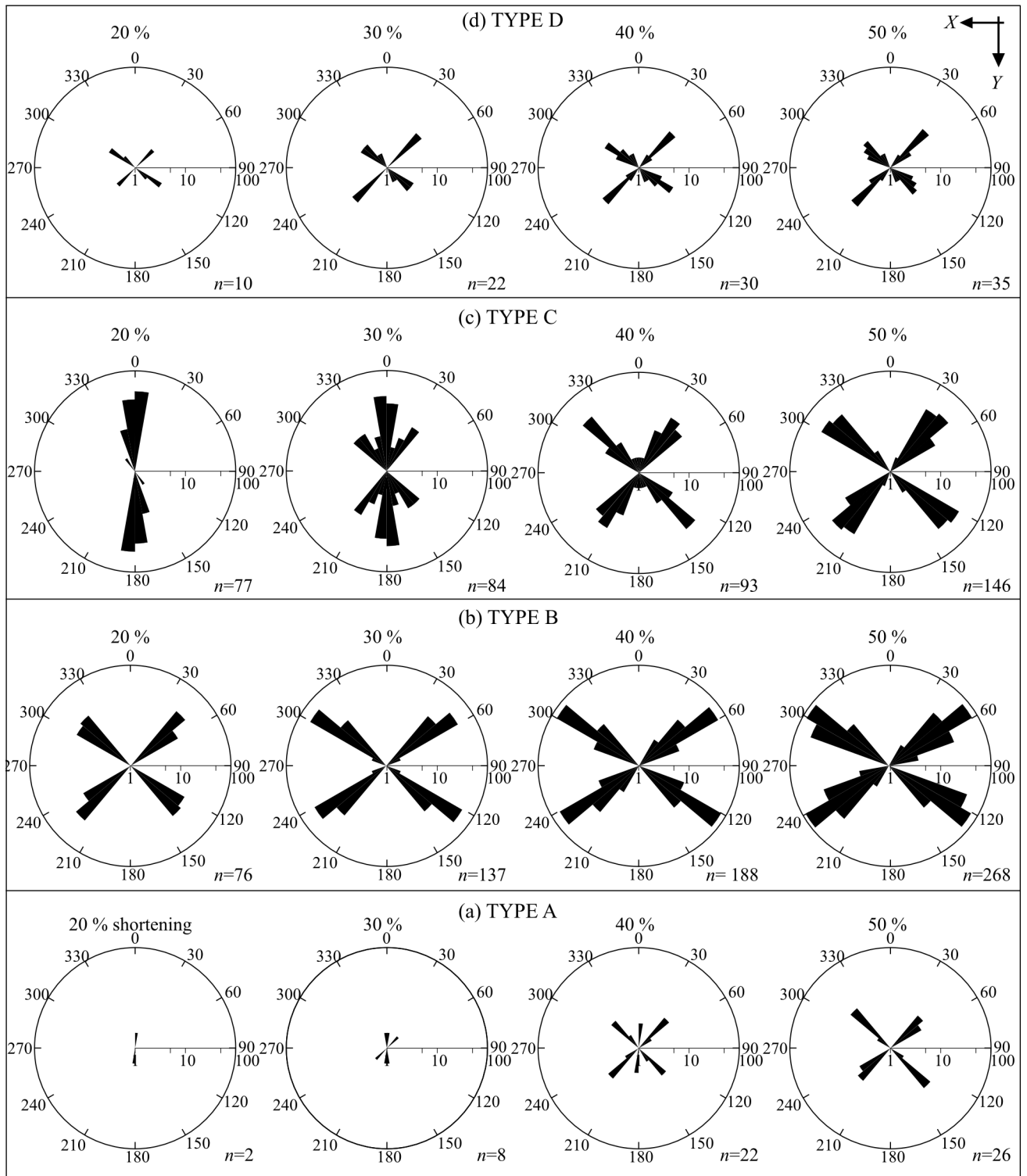
1
2 Figure 5. Photographs of the initial (0% shortening) and final (~50% shortening) stages of the
3 four multilayer models. Maps of analysed fracture networks are displayed on the right side.

1 Red dashed lines indicate reference layers. Grey shadowed areas in type D model show the
2 location of large fault zones. Only structures located in the central area of each model,
3 indicated with a rectangle, are systematically studied. I_{loc} is the localisation factor (see section
4 2.2). The degree of localisation progressively increases from model A to model D, and
5 depends on the strength, effective viscosity and degree of anisotropy of the models. Marked
6 differences between the resulting fracture networks can be clearly identified.
7



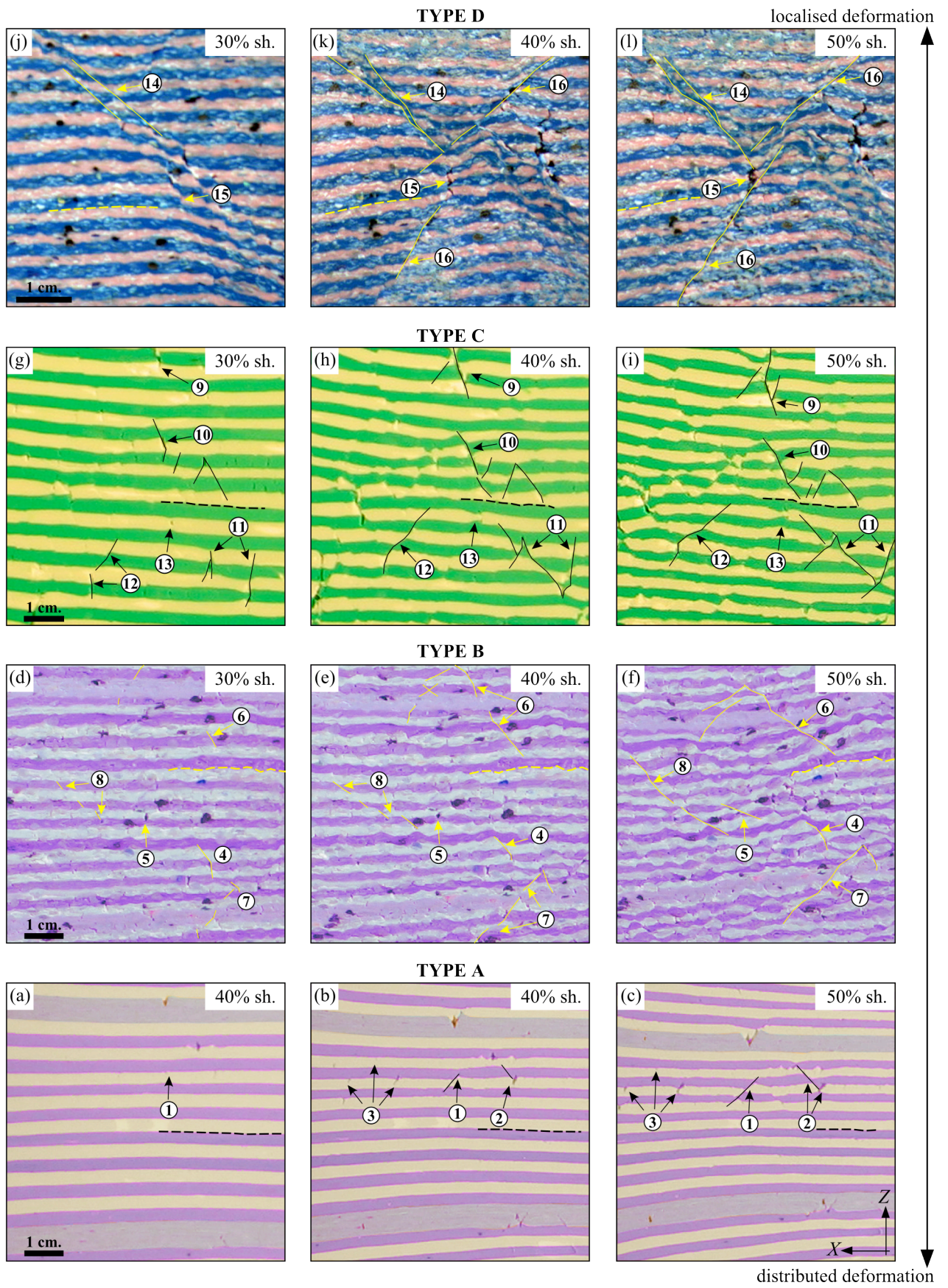
1
2
3
4
5
6

Figure 6. Stress vs. strain curves for the four multilayer experiments. Yielding followed by slight strain softening can be clearly identified for models C and D, while experiments A and B record a progressive stress increase that tends towards steady state with increasing strain.



1
2

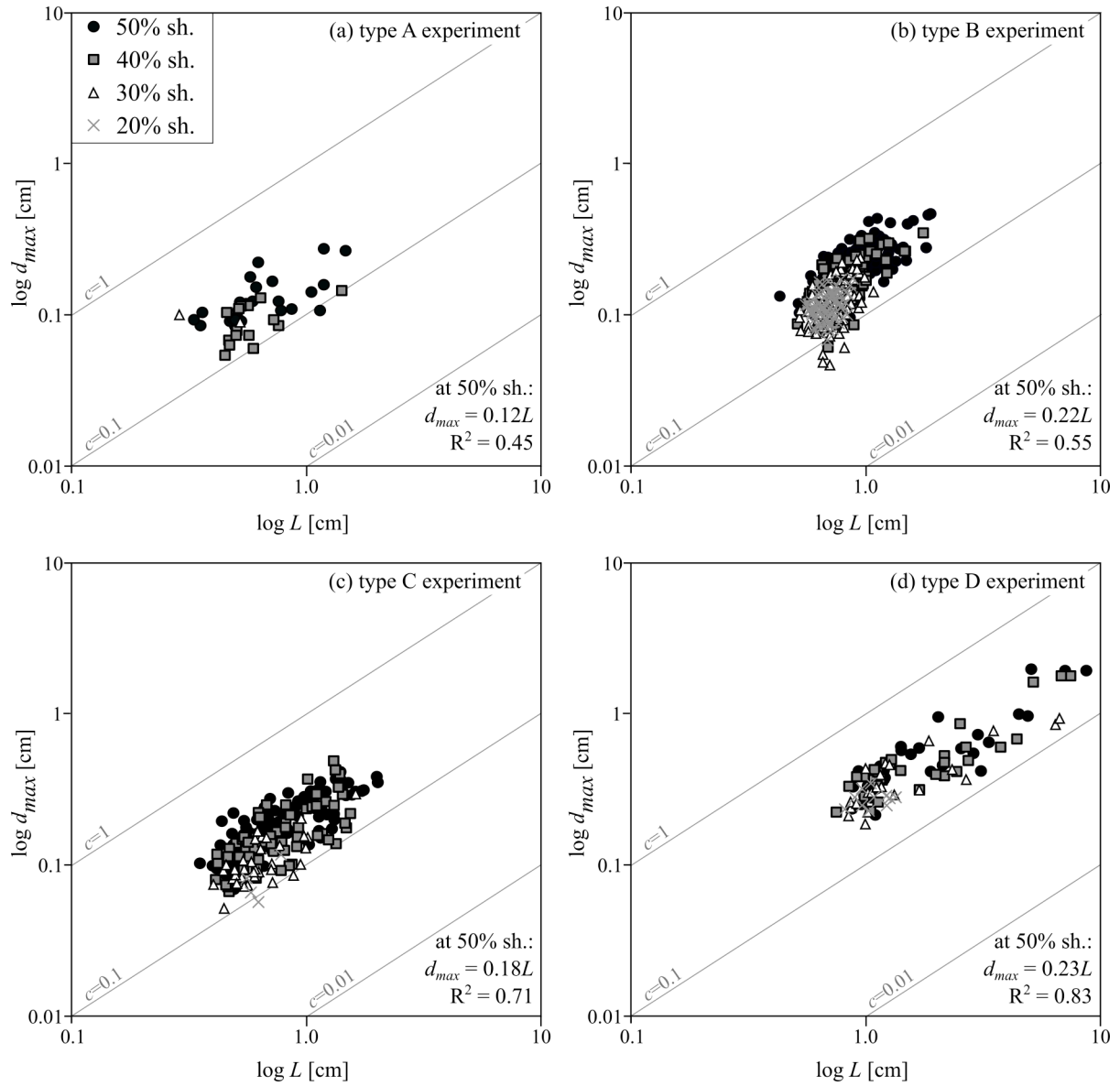
3 Figure 7. Rose diagrams showing the orientation and number of fractures (at orientation
4 intervals of 10°) of experiments: (a) type A, (b) type B, (c) type C and (d) type D. *n* is the
5 number of data measurements in each diagram. Only fractures measured within the sampling
6 area are included. Note that horizontal scales are logarithmic.



1

2

1 Figure 8. Detailed photographs showing the evolution of structures in the four different
2 experiments. (a-c) Type A experiment: (1) a shear fracture forms by collapse of a tension
3 crack; (2) coeval development of a tension crack and a shear fracture; (3) tension cracks keep
4 forming until ~40% shortening. (d-f) Type B experiment: (4) mixed-mode fracture with
5 associated drag folds. The propagation rate was very low due to plastic deformation at
6 fracture tips; (5) tension crack/void that collapsed and gave rise to a shear fracture; (6) in-
7 plane shear fracture with enhanced propagation at one of the tips; (7, 8) linkage of fracture
8 segments produced larger fractures with heterogeneous displacements. (g-i) Type C
9 experiment: (9) nucleation and propagation of a tension crack that evolved to a mixed-shear
10 mode fracture; (10) progressive enlargement of individual fractures as a result of progressive
11 tip-line propagation and linkage with the nearest fracture segments; (11) nucleation of
12 conjugate shear fractures from tension cracks, resulting in sharp fracture segments; (12)
13 relatively long shear fracture that formed by linkage of a tension crack and a shear fracture;
14 (13) small tension crack that evolved to form heterogeneous asymmetric boudinage. (j-l) Type
15 D experiment: (14) formation of two parallel dextral fractures that propagate, join and their
16 lower tip ends at a larger conjugate fracture; (15) development of a void from a tension crack
17 at the intersection between large shear fractures; (16) a very large sinistral fracture with zig-
18 zag geometry forms by segment linkage from side to side of the model. Solid lines represent
19 fractures, while dashed lines indicate layering.
20



1
2
3
4
5
6
7

Figure 9. log maximum fracture length (d_{max}) vs. log maximum fracture displacement (L) graphs for models (a) type A, (b) type B, (c) type C and (d) type D. Data correspond to shear fractures measured at 20%, 30%, 40% and 50% of shortening within the sampling area. Grey lines indicate linear relationships in the log-log graph for different c values in equation (1).